Volume 1 | Number 1 | Jan 2013 | Pages 1–100

Journal of
Materials Chemistry A

Materials for energy and sustainability
www.rsc.org/materialsA

Li⁺

ROYAL SOCIETY
OF CHEMISTRY

ROYAL SOCIETY
OF CHEMISTRY

www.rsc.org/materialsA

ARTICLE

Open Mesoporous Spherical Shell Structured Co$_3$O$_4$ with Highly Efficient Catalytic Performance in Li-O$_2$ Batteries

Fan Wang[a], Zhaoyin Wen[a],*, Chen Shen[a], Kun Rui[a], Xiangwei Wu[a] and Chunhua Chen[b]

An open mesoporous spherical shell structured (OMSS) Co$_3$O$_4$ was designed and synthesized through a two steps process. The OMSS Co$_3$O$_4$ with a diameter around 1 μm is constructed from a large number of nanoparticles mainly with (111) preferential exposed crystal planes. Superior catalytic activity for oxygen evolution reaction (OER) can be manifested in Li-O$_2$ batteries with the charge voltage platform reduced to ~3.6V. An outstanding performance of cycling stability was also achieved with a cut-off specific capacity of 1000 mAh·g^{-1} over 60 cycles. The fantastic cycling performance may be attributed to the open mesoporous spherical shell structure with high specific surface area which improves the transport capability of oxygen, increases the active sites and the sedimentary space of discharge products. It almost gets the highest cycling performance among metal oxide catalysts used in Li-O$_2$ batteries reported to date.

1 Introduction

Nowadays traditional lithium ion batteries cannot meet the stringent requirements for electric vehicles, future renewable energy storage, and other high power applications due to their low specific capacity [1, 2]. Rechargeable lithium oxygen (Li-O$_2$) batteries have therefor aroused a great deal of interests in the energy storage devices owing to their extra high theoretical specific energy density which is nearly 10 times higher than those of the commercial Li-ion batteries and exceeds those of any other existing electrochemical energy storage systems[3, 4,]. Besides, the Li-O$_2$ batteries are also environmental friendly, meeting the requirements of sustainable development. Hence the Li-O$_2$ batteries are one of the most promising energy storage candidates in the future[5-7]. Although important progress has been made in the Li-O$_2$ batteries recently[3, 8-17], significant challenges are still remained, such as large over-potentials, decomposition of electrolytes, and poor cyclability[18]. The root of those problems is mainly due to the sluggish kinetics of the oxygen evolution reaction (OER) causing high charging over-potentials, which not only result in a very low round-trip efficiency, but also short cycle life[19, 20].

The O$_2$ electrode microstructure would play an important role in determining the performance of a Li-O$_2$ battery. In order to reduce the high discharge/charge overpotentials and extend the cyclability, designing oxygen electrodes with advanced catalysts[21-29] and electrode structures have been contributed in Li-O$_2$ batteries. For example, a lot of work focused on

designing and synthesizing nanosized Co$_3$O$_4$, a promising oxide catalyst candidate in Li-O$_2$ batteries. Nanoparticles[30], nano-flakes[21, 31, 32], nano-fibers[33] etc. with high specific surface area and high catalytic activity were reported.

An air electrode of Li-O$_2$ battery should be porous for the delivery of oxygen. Generally, fabrication of the air electrode involves mixing of the catalyst particles, porous carbon and organic binder. During the mixing process, most of the catalyst particles were buried in the carbon material and those particles would not exert an effective role in the cell catalytic reaction. In addition, in order to make the catalyst particles bonded firmly, much binder should be used. However, the binder covered on the catalyst particles decreases the real catalytic surface area in the electrode, and further decrease the catalytic performance. Considering these cases, self-assembly of catalyst nanoparticles to produce a large size catalyst particles could expose more effective surface of the catalysts and reduce the dosage of binders which would enhance the catalytic activity of the air electrode. Moreover, as we well known that catalytic performance of a catalyst particle is closely related to the planes it exposed. Different planes result in different catalytic properties.

In this work, through two simple steps, we synthesize an open mesoporous spherical shell structured (OMSS) Co$_3$O$_4$ which is constructed from a large number of nanoparticles with (111) crystal planes preferentially exposed. The diameter of the microspheres is around 1 μm. When it is employed in Li-O$_2$ batteries, the Li-O$_2$ cells show an enhanced performance. The

initial charge voltage of this OMSS Co_3O_4 electrode is as low as 3.6V and the discharge capacity was more than 4200 mAh·g^{-1} at the current density of 0.1 mA·cm^{-2}. Its performance was much better than that of the Co_3O_4 nanoparticles. The most attractive improvement is the cyclability, more than 60 cycles were achieved with a cut-off specific capacity of 1000 mAh·g^{-1}, better than most of the metal oxide catalysts used in Li-O$_2$ batteries.

2 Experimental

Material preparation

All the reagents were of analytical purity and were used without further purification. The OMSS Co_3O_4 was synthesized through two simple steps as follows. In the first step, cobalt precursors were synthesized through a solvothermal process. Specifically, $Co(Ac)_2$·4H$_2$O (4 mmol, 1.019 g) was dissolved in ethylene glycol with magnetic stirring for 30 min, after then the mixture was transferred to a Teflon lined autoclave, sealed and maintained at 185 °C for 24 h. After cooled down to room temperature, the precursors were centrifuged and washed with distilled water and ethanol several times to remove any impurities. In the second step of synthesis, the as-prepared precursors (200 mg) were dispersed into deionized water (100 ml) mixed with H$_2$O$_2$ (5 ml, 30%), and then heated at 90 °C for 4 h. The final products were centrifuged, rinsed with distilled water and ethanol several times to remove any impurities, followed by subsequent drying under vacuum at 80 °C overnight. Commercial Co_3O_4 nanoparticles (Aldrich, average size ≈ 30 nm) was also used directly for comparison.

Material characterization

The crystal structure was determined by X-ray diffraction XRD with use of Rigaku Ultima diffractometer employing nickel-filtered Cu-Kα radiation (λ=1.542 Å). Morphologies of the synthesized samples were characterized with field emission scanning electron microscope (FESEM JSM-4800F) and a transmission electron microscope (TEM JEM-2100F). The surface area was determined by BET (Brunauer–Emmett–Teller) measurements using a Tristar 3000 surface area analyzer. To confirm the surface component, the X-ray photoelectron spectrum (XPS, Thermo Fisher Scientific ESCALab250) was also recorded.

Preparation of Li-O$_2$ cell and electrochemical investigation

The electrocatalytic activities of the as-prepared Co_3O_4 for the discharge and charge steps were tested in Li-O$_2$ cells. The electrodes were formed by casting a ball-milled mixture slurry of the OMSS Co_3O_4 as catalyst, Ketjen black carbon (KB) as support and polyvinylidene Fluoride (PVDF) as binder (with a weight ratio of 40:45:15) onto a nickel foam as the cathode current collector. An air electrode containing Co_3O_4 nanoparticles (Aldrich, average size ≈ 30 nm) was also prepared with the same Co_3O_4/carbon/binder ratio (40:45:15) for comparison. The as-prepared electrodes were vacuum-dried at 80 °C for 24 h. All electrodes had the similar material loadings of about 1 mg·cm^{-2} (catalyst + carbon + binder). The

electrochemical cells used were based on a Swagelok Cell design composed of a Li metal anode (14 mm in diameter, 0.25 mm in thick), an electrolyte of 1M LiTFSI in TEGDME solvent, the Celgard 2400 separator (16 mm in diameter), and the as-prepared porous cathode (14 mm in diameter). To avoid the influence of H$_2$O and CO$_2$ or any other impurities, the cells were operated at 1.5 mbar of pure O$_2$.

The galvanostatic charge and discharge tests were conducted on a LAND CT2001A battery test system at different current densities with a lower voltage limit of 2.0 V (vs. Li/Li$^+$) and upper limit of 4.2 V (vs. Li/Li$^+$), at ambient temperature after a 8 h rest period. All the specific capacities were calculated by normalizing with the mass loading of catalyst in the air electrodes.

3 Results and discussion

Physicochemical characterization of the OMSS Co_3O_4

The XRD pattern of the synthesized spherical Co_3O_4 is shown in **Fig. 1**a. All of the peaks in the XRD pattern can be indexed to the spinel Co_3O_4 (JCPDS card No. 42-1467), with no impurity peaks observed. Besides, the broadening of diffraction peaks implies the small grain size of the obtained products. Based on the Scherrer's formula $D = k\lambda / B\cos\theta$ the average particle diameter is calculated to be about 10 nm, which can also be confirmed later by TEM image (**Fig.1e**).

The morphology and microstructure of the product was further examined with scanning electron microscopy (SEM) and transmission electron microscopy (TEM). Uniformly distributed particles with a diameter of about 1μm display typical spherical shape with a hole in the middle section as
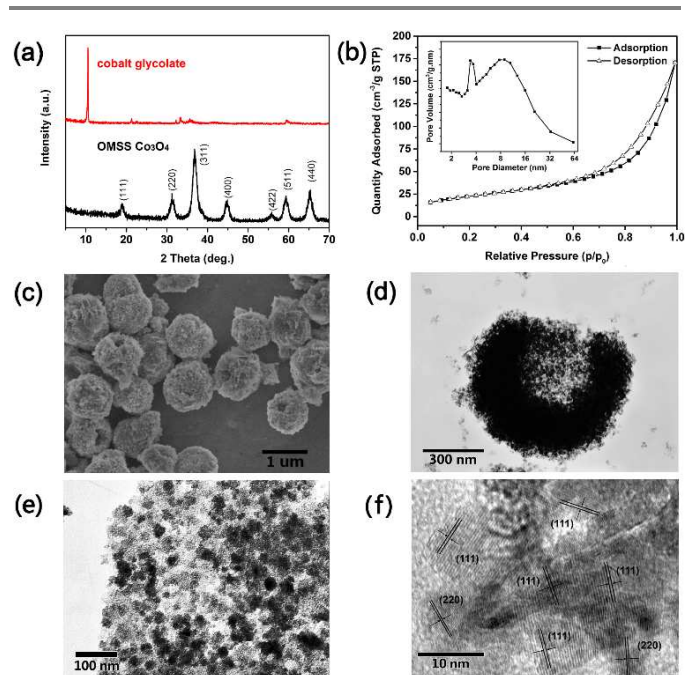

Fig. 1 XRD pattern of the prepared powder (a); typical N$_2$ gas adsorption-desorption isotherm of the Co_3O_4 products (b); SEM image (c) and TEM image (d); magnified TEM image (e) and HRTEM image (f).

shown by SEM image in **Fig. 1**c. From the TEM image (**Fig. 1**d) we can find that the products exhibit an open porous spherical shell structure with the spheres self-assembled by many nanoparticles. As can be seen from the magnified TEM image in **Fig. 1**e, those particles which construct the OMSS Co_3O_4 are around 10 nm in diameter. It well corresponds to the result of the calculation from the XRD patterns. According to the analyzed HRTEM results in **Fig. 1**f, most of nano particles can be indexed to spinel structured Co_3O_4 with corresponding planes of (111) and others can be indexed to the planes of (220).

The powder was further characterized by the N_2 adsorption-desorption experiments (**Fig .1**b). According to the IUPAC convention[34], the N_2 adsorption/desorption curves exhibit a type of IV shape with a distinct hysteresis loop observed in the range of 0.5-1.0 p/p_0, indicating a mesoporous (2-50 nm in size) feature of the as-prepared OMSS Co_3O_4.[35] The corresponding pore-size distribution (inset of **Fig.1**b) shows two peaks. As can be observed, the size of mesopores centralize on two areas with peak values of around 3.6 and 10 nm respectively. The Brunauer-Emmett-Teller (BET) surface area of the as-prepared samples is estimated to be about 83.0 $m^2 \cdot g^{-1}$, larger than that of commercial nano-Co_3O_4 (6.7 $m^2 \cdot g^{-1}$, tested by BET under the same conditions). The mesoporous sphere structure assembled by nanoparticles should have excellent adsorptive properties and also provide more reactive sites, which therefore makes it easier for oxygen transport and adsorption on the surface of the catalysts. In addition, the hollow space within the open shell with large surface area further facilitates the deposition of discharge product, thus improving the catalytic activity to a great extent.

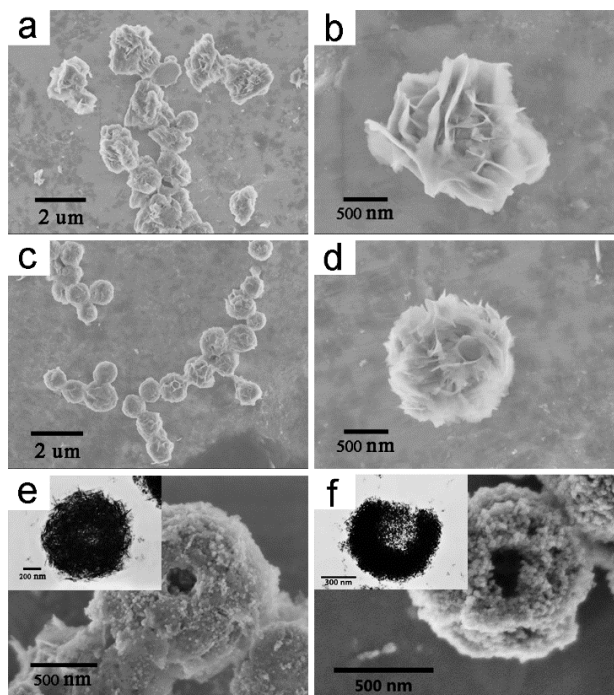**Possible formation mechanism proposed for OMSS Co_3O_4**

Fig. 2 SEM images of the products after hydrothermal reaction for 12 h (a, b) and 24 h (c, d); SEM and TEM images of the products after oxidized by H_2O_2 for 3 h (e) and 4 h (f).
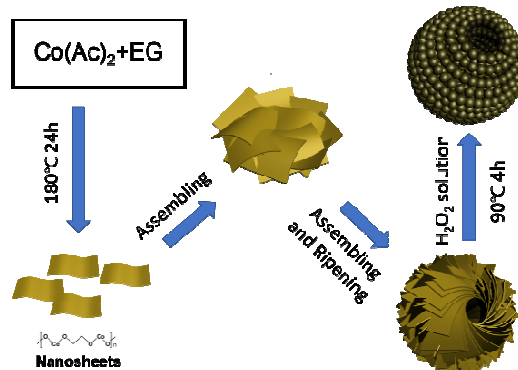

Fig. 3 Schematic illustration of the growth process of open porous spherical shell structure Co_3O_4

SEM and TEM characterizations were further involved to observe the morphology evolution during different stages of Co_3O_4 formation. The main evolving steps are schematically illustrated in **Fig. 3**, which can be ascribed to a solvothermal assembly process. Firstly, the $Co(Ac)_2$ oligomerize with glycol to form cobalt glycolate at high temperature and under high pressure, then further self-assemble into nanosheet structure through van der Waals interactions.[36] This process is comfirmed through time-dependent experiments by Xi Wang[37]. With the increase of reaction time, the cobalt glycolate oligomers nanosheets could first gradually assemble into irregular structures as shown by SEM images in **Fig. 2**a, b. By appropriately extending the reaction time, those irregular structures were found to further transform into spherical shell precursors by Ostwald mechanism[37] as can be seen from SEM results in **Fig. 2**c, d. **Fig. 1**a also shows a typical XRD pattern of the colbat precursors. The strong diffraction peak around 10° in XRD pattern is characterized as metal glycolates.[38, 39]

When it comes to the second step of synthesis, the precursors were put into H_2O_2 solution and treated at a lower temperature of 90 °C for further oxidation. During the oil bath process, cobalt glycolate sheets are oxidized into Co_3O_4 by the H_2O_2 and those precursor sheets transform into nanoparticles, eventually came into being shell structure owing to the volume effects. This morphology transition can be seen from the SEM images shown in **Fig. 2**e and f. Finally, we got the open porous spherical shell assembled by Co_3O_4 nanoparticles.

Electrochemical characterization of OMSS Co_3O_4 in Li-O_2 batteries

The electrocatalytic activity of OMSS Co_3O_4 catalyst for ORR and OER reactions in Li-O_2 cells was investigated under galvanostatic cycling conditions and compared to Co_3O_4 nanoparticles. The initial discharge capacity was measured at different current densities to characterize the rate capability of the cell (**Fig. 4**a) and a capacity as high as 1730 mAh·g^{-1} of OMSS Co_3O_4 is observed at the current density of 0.3 mA·cm^{-2}. In contrast, a much higher discharge capacity over 4200 mAh·g^{-1} than 2500 mAh·g^{-1} of nano Co_3O_4 at the current density of 0.1 mA·cm^{-2} can be obtained as **Fig. 4**b indicated, possibly owing to the increased reactive sites associated with larger surface area provided by the unique structure of open porous spherical shell. Furthermore, the discharge median voltage is found about 2.65V at the current density of 0.1 mA·cm^{-2}, while the charge process undergoes with the median voltage of 3.6 V, which is much lower than that of nano Co_3O_4. Since most reported Co_3O_4 catalysts for Li-O_2 batteries
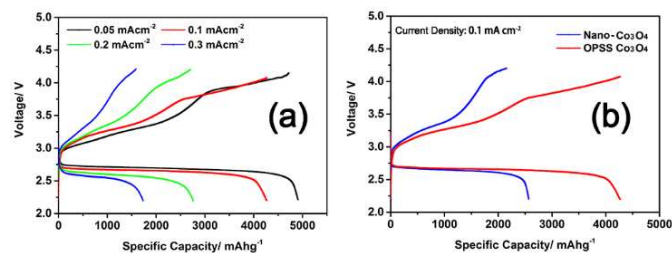
Fig. 4 (a) First galvanostatic discharge/charge curves of OMSS Co_3O_4 at different current density; (b) the first cycle of the nano-Co_3O_4 and OMSS Co_3O_4 at the current density of 0.1 mA cm^{-2}.
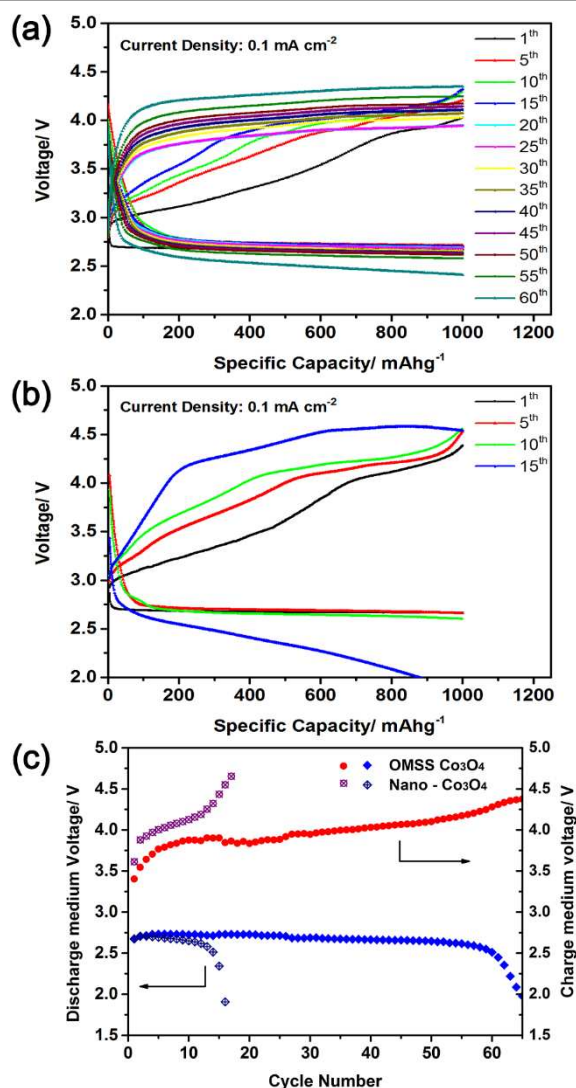

Fig.5 Discharging and charging profiles of the OMSS Co_3O_4 (a), nano-Co_3O_4 (b); the variation of discharge and charge median voltage with the cycle number (c).

delivered charge voltages above 4.0 V at the same current density[30, 40, 41], the OMSS Co_3O_4 catalyst with a very low charge voltage of 3.6 V shows its outstanding catalytic ability towards the decomposition of the discharge products Li_2O_2.

The cyclic performance of the electrode containing the OMSS Co_3O_4 was shown in **Fig. 5**a. In order to avoid a large depth of discharge and achieve improved cyclic performance of the batteries, the discharge capacities of the electrodes were limited to 1000 mAh·g^{-1}. The battery exhibited excellent cycle

stability over 60 cycles without pronounced vibration in the very stable discharge/charge curves. Moreover, the discharge and charge median voltages as a function of cycle number were also shown in **Fig. 5**c, from which we can see that the discharge median voltages of the first 26 cycles is above 2.70 V, and even after 60 cycles the voltages were still higher than 2.50 V. During charging process, the median voltage have been below 4.0 V within 36 cycles. In contrast, the battery with Co_3O_4 nanoparticles can only work for 19 cycles together with extremely high discharge voltages as shown in **Fig. 5**b.

To further get insights into the discharge and charge processes, SEM was used to detect the morphology of the oxygen electrodes. **Fig. 6** shows the SEM images of the oxygen electrode with OMSS Co_3O_4 before and after cycling in the Li-O_2 cells. **Fig. 6**a shows that the OMSS Co_3O_4 were well distributed on the primary electrode. After discharge, the discharge products Li_2O_2 could deposit inside the Co_3O_4 spherical shell as shown in **Fig. 6**c. When fully charged back, the discharge products were discovered to fully decompose with no Li_2O_2 obviously found inside and outside of the shell (**Fig. 6**d). Further evidence has been obtained from Fourier transform infrared (FTIR) with the results shown in **Fig. 7**. The peaks located at about 520 cm^{-1} and 450 cm^{-1} are the signature of Li_2O_2. After charge process, these peaks disappear which indicates that the formation and decomposition of Li_2O_2 is reversible. X-ray photoelectron spectra (XPS) was also used to investigate the discharge and charge products during the electrochemical reactions in Li-O_2 batteries. The O 1s and Li 1s XPS spectra were recorded and fitted, as shown in **Fig.8**. **Fig. 8**a (bottom spectrum) shows the O 1s XPS spectrum for the discharge cathode, from which it can be concluded that Li_2O_2 formed as the dominated discharge product[42, 43] along with some Li_2CO_3. After charge (upper spectrum), the dominated peak of Li_2O_2 disappeared indicating that the main product of Li_2O_2 can form and decompose reversibly. The Li 1s peak (**Fig. 8**b) at about 55.6 eV also indicates the main discharge product of Li_2O_2 and the reversible formation/decomposition during discharge and charge process.
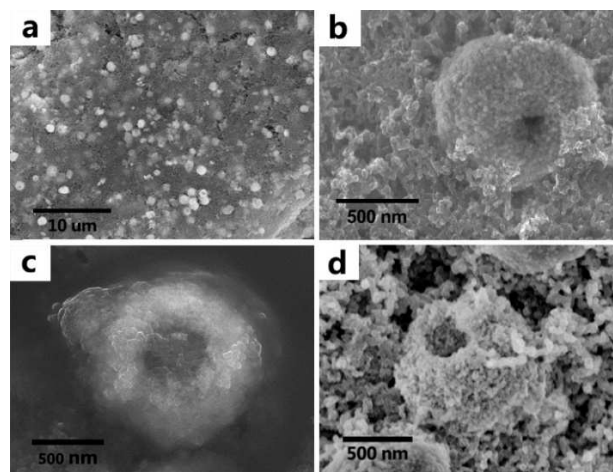

Fig. 6 SEM image of the oxygen electrode catalyzed by OMSS Co3O4: (a, b) primary electrode and OMSS Co_3O_4; (c) full discharge state; (d) full charge state.
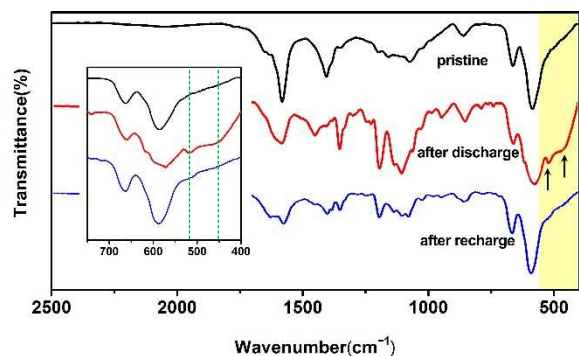
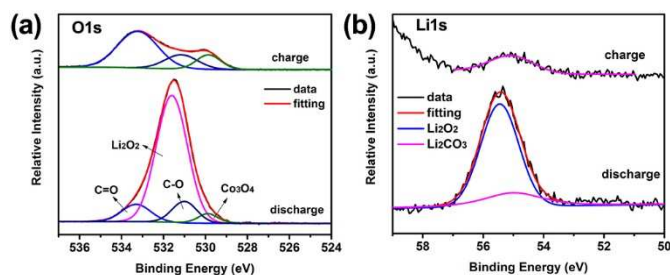**Fig. 7** FTIR spectra of the pristine cathode and after discharge, recharge in O_2.

Fig. 8 XPS spectra of (a) O 1s and (b) Li 1s peaks of the cathode after 5th discharge and charge.

The enhanced performance of the OMSS Co_3O_4 can be attributed to the unique structure features as follows. Firstly, the OMSS Co_3O_4 was composed of numerous Co_3O_4 nanoparticles (about 10 nm), whose crystal plane plays an important role in the electrochemical catalytic reaction. According to the HRTEM results of **Fig. 3**b, nanoparticles of the OMSS Co_3O_4 mainly exposed (111) plane which has been confirmed to have the highest catalytic activity for OER in Li-O_2 batteries both theoretically and experimentally[44]. Apart from the fact that Co^{3+} is more active than Co^{2+} in ORR, the (111) crystal planes contain most content of Co^{3+} relative to other planes, providing more reactive sites to facilitate OER during the charge process.[44] Secondly, the Co_3O_4 spherical shell was loose spherical shell composed of nanoparticles together with lots of mesopores confirmed by the nitrogen adsorption/desorption isotherms which could benefit the oxygen adsorption and diffusion and enhance the reaction rate on the surface of the catalysts to a certain extent. Above all, the available deposition of discharge products inside the spherical shell makes it much easier for the Li_2O_2 to be charged back together with the preservation of electrochemically available surface area.[45] In conclusion, the OMSS Co_3O_4 cathode can achieve such a long life cycle performance resulting from those merits above provided by the unique microstructure of the air electrode catalyst.

However, cycling performance of the battery after 60 cycles decreases obviously as shown in **Fig. 5**. This may be due to the decomposition of the Ketjen black carbon and the TEGDME electrolyte as well.[46-50] It has been reported that carbon is unstable on charging above 3.5 V in the presence of Li_2O_2, while Li_2CO_3 can also be formed through a side reaction during cycling[51, 52], its accumulation on cycling results in electrode passivation and capacity fading as well. So a longer cycle life is promising to be obtained further if graphene, carbon nanotube or some other carbon carrier which are more stable could be

used with the OMSS Co_3O_4 as catalyst. Anyway, our results is still better than the recent report of graphene/Co_3O_4 composite catalysts[53] with the use of Ketjen black carbon though.

4 Conclusions

In this article, we have successfully synthesized a kind of open mesoporous spherical shell structured Co_3O_4 with mainly exposed planes of (111) of high OER catalytic property. When employed as the air cathode in Li-O_2 cells, OMSS Co_3O_4 showed high efficiency in reducing the charge overpotential. Cycling performance more than 60 cycles could be achieved without pronounced vibration. The improved performance can be attributed to the exposed planes of high OER catalytic property and shell structure with abundance of sites for deposition of discharge products, avoiding severely blocking the O_2 and electrolyte transportation as long as the intact preservation of electrochemically available surface area. In a word, this structural design of the catalyst in this work indeed has exerted its effect in improving the catalytic performance in Li-O_2 cells, and making the Li-O_2 cells achieve a long life, indicating suitable utilization of such structure design for other metallic oxide catalysts in the future.

Notes and reference

[a] *CAS Key Laboratory of Materials for Energy Conversion, Shanghai Institute of Ceramics, Chinese Academy of Sciences, 1295 DingXi Road, Shanghai 200050, P. R. China.* [b] *Department of Materials Science and Engineering, University of Science and Technology of China, Hefei 230026, P. R. China. Corresponding author: Zhaoyin Wen, Fax: +86-21-52413903; Tel: +86-21-52411704; E-mail: zywen@mail.sic.ac.cn.*

1. J. M. Tarascon and M. Armand, *Nature*, 2001, **414**, 359-367.
2. T. Zhang and H. S. Zhou, *Nat. Commun.*, 2013, **4**, 7.
3. C. O. Laoire, S. Mukerjee, K. M. Abraham, E. J. Plichta and M. A. Hendrickson, *J. Phys. Chem. C*, 2009, **113**, 20127-20134.
4. P. G. Bruce, S. A. Freunberger, L. J. Hardwick and J.-M. Tarascon, *Nat. Mater.*, 2011, **11**, 19-29.
5. K. M. Abraham and Z. Jiang, *J. Electrochem. Soc.*, 1996, **143**, 1-5.
6. G. Girishkumar, B. McCloskey, A. C. Luntz, S. Swanson and W. Wilcke, *J. Phys. Chem. Lett.*, 2010, **1**, 2193-2203.
7. Z.-L. Wang, D. Xu, J.-J. Xu and X.-B. Zhang, *Chem. Soc. Rev.*, 2014, **43**, 7746-7786.
8. Y.-C. Lu, H. A. Gasteiger, M. C. Parent, V. Chiloyan and Y. Shao-Horn, *Electrochem. Solid-State Lett.*, 2010, **13**, A69.
9. J. Read, *J. Electrochem. Soc.*, 2002, **149**, A1190-A1195.
10. Y.-C. Lu, Z. Xu, H. A. Gasteiger, S. Chen, K. Hamad-Schifferli and Y. Shao-Horn, *J. Am. Chem. Soc.*, 2010, **132**, 12170-12171.
11. Y. M. Cui, Z. Y. Wen and Y. Liu, *Energy Environ. Sci.*, 2011, **4**, 4727-4734.
12. Y. C. Lu, H. A. Gasteiger and Y. Shao-Horn, *J. Am. Chem. Soc.*, 2011, **133**, 19048-19051.
13. T. Zhang and H. S. Zhou, *Nat Commun*, 2013, **4**, 1817.

14. T. Ogasawara, A. Débart, M. Holzapfel, P. Novák and P. G. Bruce, *J. Am. Chem. Soc.*, 2006, **128**, 1390-1393.
15. F. Wang, C. S. Liang, D. L. Xu, H. Q. Cao, H. Y. Sun and Z. K. Luo, *J. Inorg. Mater.*, 2012, **27**, 1233-1242.
16. J.-J. Xu, D. Xu, Z.-L. Wang, H.-G. Wang, L.-L. Zhang and X.-B. Zhang, *Angew. Chem. Int. Ed.*, 2013, **52**, 3887-3890.
17. J.-J. Xu, Z.-L. Wang, D. Xu, F.-Z. Meng and X.-B. Zhang, *Energy Environ. Sci.*, 2014, **7**, 2213-2219.
18. J. Lu, L. Cheng, K. C. Lau, E. Tyo, X. Luo, J. Wen, D. Miller, R. S. Assary, H.-H. Wang, P. Redfern, H. Wu, J.-B. Park, Y.-K. Sun, S. Vajda, K. Amine and L. A. Curtiss, *Nat Commun*, 2014, **5**.
19. Z. Q. Peng, S. A. Freunberger, Y. H. Chen and P. G. Bruce, *Science*, 2012, **337**, 563-566.
20. M. Park, H. Sun, H. Lee, J. Lee and J. Cho, *Adv. Energy Mater.*, 2012, **2**, 780-800.
21. G. Y. Zhao, J. X. Lv, Z. M. Xu, L. Zhang and K. N. Sun, *J. Power Sources*, 2014, **248**, 1270-1274.
22. C. S. Park, J. H. Kim and Y. J. Park, *J. Electroceram.*, 2013, **31**, 224-230.
23. T. H. Yoon and Y. J. Park, *Nanoscale Res. Lett.*, 2012, **7**, 1-4.
24. Y. Qin, J. Lu, P. Du, Z. H. Chen, Y. Ren, T. P. Wu, J. T. Miller, J. G. Wen, D. J. Miller, Z. C. Zhang and K. Amine, *Energy Environ. Sci.*, 2013, **6**, 519-531.
25. T. T. Truong, Y. Z. Liu, Y. Ren, L. Trahey and Y. G. Sun, *ACS Nano*, 2012, **6**, 8067-8077.
26. Y. Cao, Z. K. Wei, J. He, J. Zang, Q. Zhang, M. S. Zheng and Q. F. Dong, *Energy Environ. Sci.*, 2012, **5**, 9765-9768.
27. Y. Cao, Z. Wei, J. He, J. Zang, Q. Zhang, M. Zheng and Q. Dong, *Energy Environ. Sci.*, 2012, **5**, 9765-9768.
28. J. Q. Zhang, G. L. Chen, M. Z. An and P. Wang, *Int. J. Electrochem. Sci.*, 2012, **7**, 11957-11965.
29. R. Choi, J. Jung, G. Kim, K. Song, Y. I. Kim, S. C. Jung, Y. K. Han, H. Song and Y. M. Kang, *Energy Environ. Sci.*, 2014, **7**, 1362-1368.
30. C. W. Sun, F. Li, C. Ma, Y. Wang, Y. L. Ren, W. Yang, Z. H. Ma, J. Q. Li, Y. J. Chen, Y. Kim and L. Q. Chen, *J. Mater. Chem. A*, 2014, **2**, 7188-7196.
31. G. Y. Zhao, Z. M. Xu and K. N. Sun, *J. Mater. Chem. A*, 2013, **1**, 12862-12867.
32. Q.-c. Liu, J.-j. Xu, Z.-w. Chang and X.-b. Zhang, *J. Mater. Chem. A*, 2014, **2**, 6081-6085.
33. W. H. Ryu, T. H. Yoon, S. H. Song, S. Jeon, Y. J. Park and I. D. Kim, *Nano Lett.*, 2013, **13**, 4190-4197.
34. S. J. Gregg, K. S. W. Sing and H. Salzberg, *J. Electrochem. Soc.*, 1967, **114**, 279C-279C.
35. D. V. Bavykin, V. N. Parmon, A. A. Lapkin and F. C. Walsh, *J. Mater. Chem.*, 2004, **14**, 3370-3377.
36. F. Tao, C. Gao, Z. Wen, Q. Wang, J. Li and Z. Xu, *J. Solid State Chem.*, 2009, **182**, 1055-1060.
37. X. Wang, X.-L. Wu, Y.-G. Guo, Y. Zhong, X. Cao, Y. Ma and J. Yao, *Adv. Funct. Mater.*, 2010, **20**, 1680-1686.
38. X. Jiang, Y. Wang, T. Herricks and Y. Xia, *J. Mater. Chem.*, 2004, **14**, 695-703.
39. D. Q. Liu, X. Wang, X. B. Wang, W. Tian, Y. Bando and D. Golberg, *Sci Rep*, 2013, **3**, 2543.
40. T. H. Yoon and Y. J. Park, *J. Power Sources*, 2013, **244**, 344-353.
41. C. S. Park, K. S. Kim and Y. J. Park, *J. Power Sources*, 2013, **244**, 72-79.
42. J. Lu, Y. Qin, P. Du, X. Y. Luo, T. P. Wu, Y. Ren, J. G. Wen, D. J. Miller, J. T. Miller and K. Amine, *RSC Adv.*, 2013, **3**, 8276-8285.
43. Y. Lei, J. Lu, X. Luo, T. Wu, P. Du, X. Zhang, Y. Ren, J. Wen, D. J. Miller, J. T. Miller, Y.-K. Sun, J. W. Elam and K. Amine, *Nano Lett.*, 2013, **13**, 4182-4189.
44. D. Su, S. Dou and G. Wang, *Sci. Rep.*, 2014, **4**.
45. J.-J. Xu, Z.-L. Wang, D. Xu, L.-L. Zhang and X.-B. Zhang, *Nat Commun*, 2013, **4**, 2438.
46. M. M. O. Thotiyl, S. A. Freunberger, Z. Q. Peng and P. G. Bruce, *J. Am. Chem. Soc.*, 2013, **135**, 494-500.
47. A. Debart, A. J. Paterson, J. Bao and P. G. Bruce, *Angew. Chem. Int. Edit.*, 2008, **47**, 4521-4524.
48. B. D. McCloskey, A. Speidel, R. Scheffler, D. C. Miller, V. Viswanathan, J. S. Hummelshøj, J. K. Nørskov and A. C. Luntz, *J. Phys. Chem. Lett.*, 2012, **3**, 997-1001.
49. D. Xu, Z. L. Wang, J. J. Xu, L. L. Zhang and X. B. Zhang, *Chem. Commun.*, 2012, **48**, 6948-6950.
50. Z.-L. Wang, D. Xu, J.-J. Xu, L.-L. Zhang and X.-B. Zhang, *Adv. Funct. Mater.*, 2012, **22**, 3699-3705.
51. B. D. McCloskey, D. S. Bethune, R. M. Shelby, G. Girishkumar and A. C. Luntz, *J. Phys. Chem. Lett.*, 2011, **2**, 1161-1166.
52. S. A. Freunberger, Y. Chen, N. E. Drewett, L. J. Hardwick, F. Bardé and P. G. Bruce, *Angew. Chem. Int. Ed.*, 2011, **50**, 8609-8613.
53. C. Sun, F. Li, C. Ma, Y. Wang, Y. Ren, W. Yang, Z. Ma, J. Li, Y. Chen, Y. Kim and L. Chen, *J. Mater. Chem. A*, 2014, **2**, 7188-7196.